Nano Research 2018, 11(12): 6252–6259
https://doi.org/10.1007/s12274-018-2148-z
Research Article
ISSN 1998-0124
CN 11-5974/O4

Probing magnetic-proximity-effect enlarged valley splitting in monolayer WSe_2 by photoluminescence

Chenji Zou[1,2], Chunxiao Cong[3] (✉), Jingzhi Shang[2], Chuan Zhao[4], Mustafa Eginligil[5], Lishu Wu[2], Yu Chen[2], Hongbo Zhang[2], Shun Feng[2], Jing Zhang[2], Hao Zeng[4] (✉), Wei Huang[1,5] (✉), and Ting Yu[2] (✉)

[1] *Shaanxi Institute of Flexible Electronics (SIFE), Northwestern Polytechnical University (NPU), 127 West Youyi Road, Xi'an 710072, China*
[2] *Division of Physics and Applied Physics, School of Physical and Mathematical Sciences, Nanyang Technological University, 21 Nanyang Link, Singapore 637371, Singapore*
[3] *State Key Laboratory of ASIC & System, School of Information Science and Technology, Fudan University, Shanghai 200433, China*
[4] *Department of Physics, University at Buffalo, State University of New York, Buffalo, New York 14260, USA*
[5] *Key Laboratory of Flexible Electronics (KLOFE) & Institute of Advanced Materials (IAM), Jiangsu National Synergetic Innovation Centre for Advanced Materials (SICAM), Nanjing Tech University (NanjingTech), 30 South Puzhu Road, Nanjing 211816, China*

Received: 5 April 2018
Revised: 25 June 2018
Accepted: 9 July 2018

KEYWORDS

valley splitting, transition metal dichalcogenides, magnetic proximity effect, heterostructure, magnetic exchange field

ABSTRACT

Possessing a valley degree of freedom and potential in information processing by manipulating valley features (such as valley splitting), group-VI monolayer transition metal dichalcogenides have attracted enormous interest. This valley splitting can be measured based on the difference between the peak energies of σ^+ and σ^- polarized emissions for excitons or trions in direct band gap monolayer transition metal dichalcogenides under perpendicular magnetic fields. In this work, a well-prepared heterostructure is formed by transferring exfoliated WSe_2 onto a EuS substrate. Circular-polarization-resolved photoluminescence spectroscopy, one of the most facile and intuitive methods, is used to probe the difference of the gap energy in two valleys under an applied out-of-plane external magnetic field. Our results indicate that valley splitting can be enhanced when using a EuS substrate, as compared to a SiO_2/Si substrate. The enhanced valley splitting of the WSe_2/EuS heterostructure can be understood as a result of an interfacial magnetic exchange field originating from the magnetic proximity effect. The value of this magnetic exchange field, based on our estimation, is approximately 9 T. Our findings will stimulate further studies on the magnetic exchange field at the interface of similar heterostructures.

1 Introduction

Monolayer (ML) transition metal dichalcogenides (TMDs) with the chemical formula MX_2 (e.g., M = Mo, W; X = S, Se) have attracted enormous attention in nanoelectronics and optoelectronics for their novel

Address correspondence to Ting Yu, yuting@ntu.edu.sg; Chunxiao Cong, cxcong@fudan.edu.cn; Hao Zeng, haozeng@buffalo.edu; Wei Huang, iamwhuang@nwpu.edu.cn

properties in both fundamental studies and potential applications [1–6]. Unlike gapless graphene [7], ML MX_2 are semiconductors with a direct band gap in the visible spectrum. There are two energy-degenerate valleys *K* and *K*′ located at the corners of the Brillouin zone in ML MX_2 [8, 9]. Because of breaking of inversion symmetry in ML TMDs [10, 11], the two valleys are inequivalent, with different orbital magnetic moments, and exhibit valley-selective circular dichroism behavior [11–13]. Thus, it is possible to manipulate the valley degree of freedom, which can be utilized in future valleytronic devices [14, 15].

Valley physics in ML TMDs can be studied using circular-polarization-resolved photoluminescence (PL) spectroscopy under an external magnetic field [16, 17]. In addition to valley polarization, valley degeneracy can be lifted by applying an out-of-plane external magnetic field, because the external magnetic field breaks the time-reversal symmetry [17, 18]. Previously, valley splitting was observed by applying large magnetic fields to $MoSe_2$ (10 T) [18], $MoTe_2$ (29 T) [19], WSe_2 (30 T) [20], and MoS_2 and WS_2 (65 T) [21] on SiO_2/Si substrates. Although these studies are very important (even pioneering), these large magnetic fields are not practical for valleytronic device applications. Intuitively, a well-prepared heterostructure consisting of ML TMD on a magnetic substrate can lead to enhanced valley splitting based on the interfacial magnetic exchange field (MEF). For two-dimensional materials, this MEF was first revealed in the EuS/graphene heterostructure [22], and later, was realized for CVD-grown ML WSe_2 on a ferromagnetic EuS substrate, in which a valley splitting of 2.5 meV for A excitons was obtained at only 1 T using magneto-reflectance measurements [23]. This remarkable valley splitting is induced by the MEF at the heterostructure interface due to the magnetic proximity effect.

Here, considering the unique advantages of strong light emission from these 2D semiconductors, we conduct systematic circular-polarization-resolved magneto-PL measurements in exfoliated ML WSe_2 on a ferromagnetic substrate of EuS and on a nonmagnetic substrate (NMS) of SiO_2/Si. For ML WSe_2 on the nonmagnetic SiO_2/Si, the valley splittings (as a function of the applied magnetic field of both A excitons and trions) are linear and show no saturation in the applied magnetic field range. In contrast, for ML WSe_2 on EuS, the valley splittings of both A excitons and trions dramatically increase with increasing magnetic field when $|B| < 1$ T, which is different from the case of ML WSe_2 on SiO_2/Si. For larger magnetic fields, i.e., $|B| > 1$ T, the valley splittings of A excitons and trions continue to increase, but at a much lower rate (the rate is very similar to the case of ML WSe_2 on SiO_2/Si). The enhanced valley splittings of both A excitons and trions in ML WSe_2 on the ferromagnetic substrate EuS are due to an interfacial MEF, resulting from the magnetic proximity effect. These results demonstrate that the valley splitting of ML WSe_2 can be controlled by the magnetic properties of the substrate, which is beneficial for future valleytronic devices.

2 Results and discussion

The valley physics of ML TMDs has recently become one of the hottest topics in condensed matter physics. The breaking of inversion symmetry creates two degenerate but inequivalent *K* and *K*′ valleys in ML TMDs. Figure 1(a) presents the valley selection rule for an A exciton. For the *K* valley, only electrons with spin-up can be excited from the upper valence band to the upper conduction band, whereas electrons with spin-down can be excited from the lower valence band to the lower conduction band, based on giant spin-orbit coupling [24]. The situation is the opposite in the *K*′ valley, because of spin-valley locking. In the absence of an external magnetic field, the two valleys are degenerate. However, when an external magnetic field *B* is applied, the degeneracy of these two valleys is lifted, which can be understood as follows. The A exciton energy is given by $E_{X_0} = E_C - E_V - E_B$, where E_C and E_V are conduction band edge and valence band edge, respectively, and E_B is the binding energy of the A exciton. As is known, σ^+ polarized light can excite electrons in the *K* valley, whereas σ^- polarized light can excite electrons in the *K*′ valley. Therefore, the A exciton energy excited by σ^+ polarized light can be written as $E^+_{X_0} = E^+_C - E^+_V - E_B$. A exciton energy excited by σ^- polarized light can be written as $E^-_{X_0} = E^-_C - E^-_V - E_B$. Note that E_B remains the same in the two cases. Therefore, the valley splitting is given by $\Delta E = E^+_{X_0} - E^-_{X_0} = E^+_C - E^-_C - (E^+_V - E^-_V)$. Because the

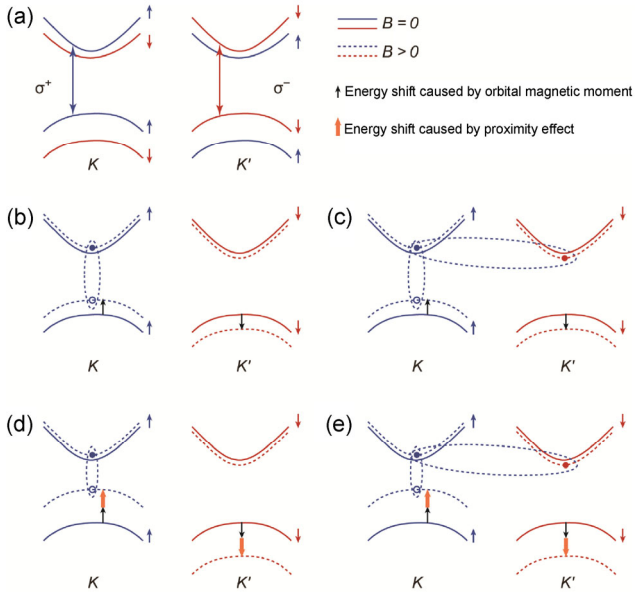

Figure 1 Valley selection rules and valley splitting for K and K' valleys in monolayer WSe_2. (a) Valley selection rules of σ^+ and σ^- excitation for an A exciton are presented. The blue (red) vertical lines show transitions of spin-up (-down) electrons in K (K') valleys by σ^+ (σ^-) excitation. (b) Valley splitting of A excitons in WSe_2 on a nonmagnetic substrate has only contribution from the atomic orbital magnetic moment in the valence band represented by the black arrow. (c) Valley splitting of trions in WSe_2 on a nonmagnetic substrate, which consists of an A exciton in the K valley and an electron in the K' valley. (d) Valley splitting of A excitons in WSe_2 on a magnetic substrate has an additional contribution due to magnetic exchange field ΔE_{MEF}, represented by the thick orange arrow. (e) Similarly, valley splitting of trions in WSe_2 on a magnetic substrate also has the additional element (ΔE_{MEF}) due to the magnetic exchange field.

valence band edge and the conduction band edge possess different magnetic moments, there will be a different energy shift when an out-of-plane magnetic field is applied. Thus $\Delta E = E_C^+ - E_C^- - (E_V^+ - E_V^-) = -(\mu^C - \mu^V)B$ [18]. Here, μ^C and μ^V are the total magnetic moments of the conduction and valence bands, respectively. The total magnetic moments consist of the magnetic moments due to orbital, carrier spin, and delocalized Bloch wave-functions in the valence band and the conduction band.

In the case of A excitons on a NMS such as SiO_2/Si, the only non-zero contribution comes from the orbital magnetic moment in the valence band, which is $-2\mu_B$ in the K valley (indicated by the black arrow in Fig. 1(b)). Meanwhile, there is another $+2\mu_B$ in the K' valley, and thus, the total valley splitting of A excitons on a nonmagnetic substrate (NMSE) is $\Delta E_{NMSE} = -4\mu_B B$ [17–21, 25]. In the case of a σ^+ polarized trion, which consists of an A exciton in the K valley and an electron in the K' valley–intervalley trion (see Fig. 1(c)), the extra electron contribution in the K' valley should be considered, in addition to $-2\mu_B$ of the A exciton case. However, when calculating the total valley splitting of σ^+ and σ^- polarized trions, the contributions of the extra electrons under the σ^+ and σ^- configurations cancel each other. As a result of the cancellation, the valley splitting of trions on a nonmagnetic substrate (NMST) is also $\Delta E_{NMST} = -4\mu_B B$ [17].

The case of A excitons in a ML TMD on a magnetic substrate is shown in Fig. 1(d). The valley splitting of A excitons now has an additional element (ΔE_{MEF}) because of the MEF induced by the magnetic proximity effect. The contribution of the externally applied magnetic field ΔE_{MSE} is expected to be the same as that of the nonmagnetic case ΔE_{NMSE}. Thus, the total valley splitting of A excitons (TE) is $\Delta E_{TE} = \Delta E_{MSE} + \Delta E_{MEF}$. As shown in Fig. 1(e), for an intervalley trion consisting of an A exciton in the K valley and an electron in the K' valley, the contribution to the valley splitting of an external magnetic field, ΔE_{MST} is the same as ΔE_{NMST}. Then, considering the contribution of MEF, the total valley splitting of trions (TT) on a magnetic substrate is $\Delta E_{TT} = \Delta E_{MST} + \Delta E_{MEF}$.

The flakes of WSe_2 were mechanically exfoliated from WSe_2 crystals onto a SiO_2/Si substrate and a EuS substrate grown using e-beam evaporation. Optical microscope images of the samples are shown in Figs. 2(a) and 2(b). The encircled area shows the monolayer WSe_2; the corresponding PL mapping images are shown in Figs. 2(c) and 2(d). A detailed experimental setup for magneto-PL measurements is illustrated in Fig. 2(e); a polarizer and a quarter wave plate are used to generate either σ^+ or σ^- excitation. At top of the optical head, another polarizer is used to detect σ^+ or σ^- emission signals. Throughout the measurements, a laser beam of 2.33 eV photon energy is focused on a ~ 1 μm spot, with a power of 700 μW. The sample is placed on a cryogenic sample holder at 4.2 K so that the magnetic field can be applied perpendicular to the sample (i.e., the Faraday geometry). Raman spectra acquired at 4.2 K are shown in Fig. 2(f). There are two peaks in the range of 251 to 265 cm^{-1} for

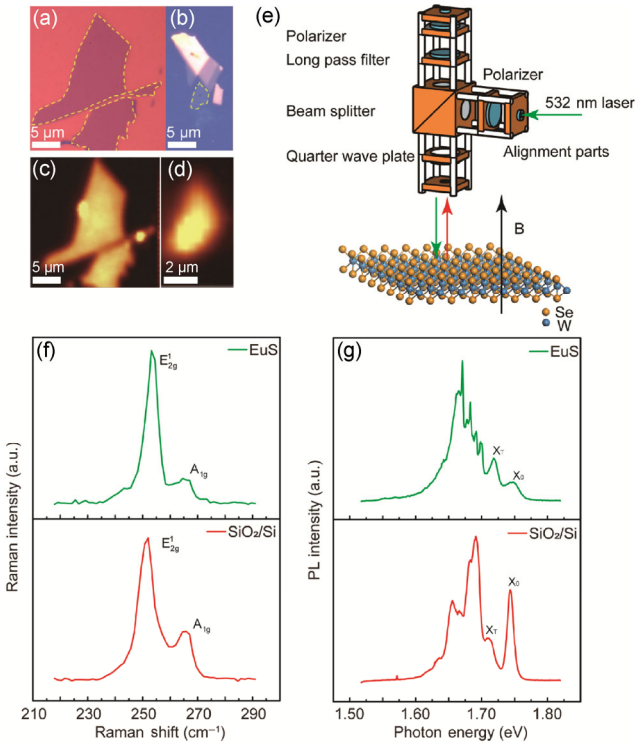

Figure 2 Raman and photoluminescence of monolayer WSe_2 on SiO_2/Si and EuS substrates without an applied magnetic field and experimental setup for circular-polarization-resolved magneto-PL measurements. Optical microscope images of ML WSe_2 on (a) SiO_2/Si, (b) EuS substrate and corresponding PL mapping images at zero field on (c) SiO_2/Si and (d) EuS. (e) Schematic setup of the circular-polarization-resolved magneto-PL measurement. A polarizer and a quarter wave plate are used to generate either σ^+ or σ^- excitation. At top of optical head, another polarizer is used in order to detect σ^+ or σ^- emission signal. (f) Raman spectra of ML WSe_2 on SiO_2/Si and EuS substrates. There are two peaks around 251 and 265 cm^{-1}, which correspond to E^1_{2g} and A_{1g} modes, respectively. (g) PL spectra of ML WSe_2 on SiO_2/Si and EuS substrates excited by a 532 nm laser show A exciton (X_0) and trion (X_T) emission peaks.

WSe_2 on both SiO_2/Si and EuS, which correspond to E^1_{2g} and A_{1g} modes, respectively. Based on the previous reports, our WSe_2 samples are confirmed to be monolayer samples [26, 27]. For ML WSe_2 on the EuS substrate, E^1_{2g} exhibits blue shift compared with that on SiO_2/Si, which is probably due to the compressive strain of the interfacial surface [28, 29], because E^1_{2g} is sensitive to strain. For WSe_2 on EuS, the thermal expansion coefficient of EuS is larger than that of WSe_2 [30, 31], which results in compressive strain between the surface when cooling the heterostructure to cryogenic temperatures. However, for WSe_2 on SiO_2/Si, this strain can be neglected because the thermal expansion coefficient of SiO_2 is very close to that of WSe_2 [32]. Additionally, the charge transfer process between EuS and WSe_2, which increases the electron doping level in WSe_2, broadens the width of the A_{1g} mode because of the strong electron-phonon coupling of the A_{1g} mode [33]. Figure 2(g) shows the PL spectra of WSe_2 on both substrates at 4.2 K for zero applied magnetic field. For WSe_2 on SiO_2/Si, the peaks around 1.74 and 1.71 eV are due to A excitons (X_0) and trions (X_T), respectively. Here, the A exciton peak is more pronounced than the trion peak, whereas for WSe_2 on EuS, the trion peak is dominant. This phenomenon can be explained by considering the heterostructure formed by WSe_2 and EuS. EuS is a ferromagnetic material with a work function of 3.3 eV [34], whereas the work function of ML WSe_2 is 4.3 eV [35]. Therefore, in the heterostructure, a charge transfer process takes place, i.e., electrons transfer from EuS to WSe_2 because of the higher work function of WSe_2 [36]. These electrons facilitate the formation of more trions in WSe_2; therefore, the trion emission peak is dominant in the spectra because of the higher doping level, as compared to the SiO_2/Si substrate case.

To investigate the valley splitting of ML WSe_2 on nonmagnetic SiO_2/Si and ferromagnetic EuS substrates, circular-polarization-resolved magneto-PL measurements were conducted.

For WSe_2 on SiO_2/Si, in the absence of an external magnetic field, there is no valley splitting between σ^+ and σ^- emissions, as shown in Fig. 3(a). Note that the peak near 1.71 eV is due to trion emission, whereas the peak near 1.74 eV is due to A excitons [37–40]. When the magnetic field is increased to 7 T, there is energy splitting between σ^+ and σ^- emissions. The magnetic field suppresses the trion peak intensity under the σ^+ configuration (blue curve), whereas for the A exciton peak, the intensity of σ^+ emission is slightly stronger than that of σ^- emission. When applying −7 T, the results are reversed, i.e., the trion peak intensity under the σ^- configuration (red curve) is suppressed and the A exciton peak intensity of σ^- emission is slightly stronger than that of σ^+ emission. A previous report showed, that the valley polarization of A exciton emission is mainly dependent on the initially-optically-created valley polarization, rather than being influenced

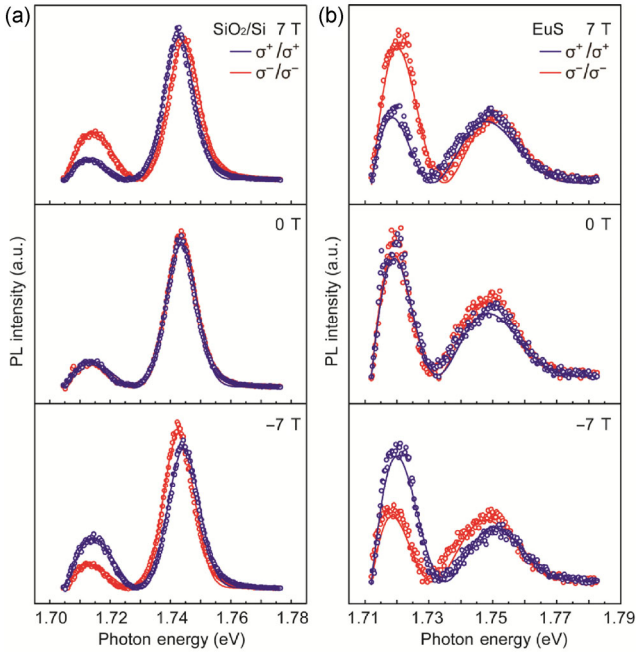

Figure 3 Magneto-PL spectra of WSe_2 on SiO_2/Si and EuS substrates at selected magnetic fields. Circularly polarized magneto-PL spectra of WSe_2 on (a) nonmagnetic SiO_2/Si and (b) ferromagnetic EuS under magnetic fields of −7 T, 0 T, and 7 T are presented. The blue (red) curves are defined as emission collected of σ^+ (σ^-) polarized light where the sample is excited by σ^+ (σ^-) polarized light. Open circles are original collected data, all spectra are presented by subtracting the background spectrum.

by the magnetic field [25]. Our results show that the valley polarization of A exciton emission is slightly sensitive to the magnetic field, which was also found in the literature [16]. For the valley polarization of trion emissions, it is also dependent on the magnetic field, in addition to the initially-optically-created valley polarization. The different valley polarization behaviors between A exciton and trion emissions from ML WSe_2 are probably due to the fact that the PL emission time of the trion is much longer than that of the A exciton [25].

The same measurements were also conducted for WSe_2 on the magnetic EuS, which can be seen in Fig. 3(b). At zero field, the peak near 1.72 eV arises from trion emission, whereas the peak near 1.75 eV is due to A excitons. There is a blue shift for both A exciton emission and trion emission, as compared to that of ML WSe_2 on SiO_2/Si at zero field. This phenomenon is probably due to the compressive strain between ML WSe_2 and EuS [41, 42], which confirms our Raman results. Another interesting feature is that the trion emission intensity is stronger than that of the A exciton emission intensity at zero field, which is due to the charge transfer process, as discussed above. The PL spectra acquired at 7 T and −7 T show energy splitting between σ^+ and σ^- emission, which are similar to that of ML WSe_2 on the SiO_2/Si substrate, albeit with larger magnitude.

To elaborate on the valley splitting enhancement of ML WSe_2 on EuS, valley splittings of A excitons in ML WSe_2 on SiO_2/Si and EuS are plotted as a function of the magnetic field in Fig. 4(a). The red squares are collected from ML WSe_2 on SiO_2/Si. These data show a linear relationship with magnetic field with a slope of −0.23 meV/T for A excitons; the associated effective g-factor can be extracted as 3.97, which is in agreement with previous reports (see Table 1) [16, 23, 25, 37]. For valley splitting data collected from ML WSe_2 on EuS (black squares in Fig. 4(a)), we observe for small magnetic fields, i.e., $|B| < 1$ T, that the absolute value of the valley splitting dramatically increases for a non-zero magnetic field, reaching up to 2.4 meV at −1 T. This valley splitting has two components, one is induced by the external magnetic field (ΔE_{MSE}), and the other is induced by the MEF (ΔE_{MEF}). Thus, the total valley splitting can be expressed as $-g\mu_B(B+B')$. Here, B' is the MEF and B is the externally applied field. We assume that the effective g-factor of the A excitons in ML WSe_2 on EuS is the same as that on the SiO_2/Si substrate, which is theoretically 4. In this case, the MEF can be roughly estimated as $B' = -\dfrac{\Delta E}{g\mu_B} - B$. Hence, the value of MEF in our case is approximately 9 T. Note that the MEF is a short-range field induced by the magnetic proximity effect, which means it is strongly influenced by the interface between WSe_2 and EuS. Our estimated MEF is slightly smaller than that in the previous report [23]. This difference might be caused by both sample preparation and the post-annealing process.

To explore the influence of MEF on trion emission, valley splittings of trions in ML WSe_2 on SiO_2/Si and EuS are plotted as a function of the magnetic field, as shown in Fig. 4(b). The red dots are collected from ML WSe_2 on SiO_2/Si. Similar to the A exciton case, the valley splitting of trions shows a linear relationship

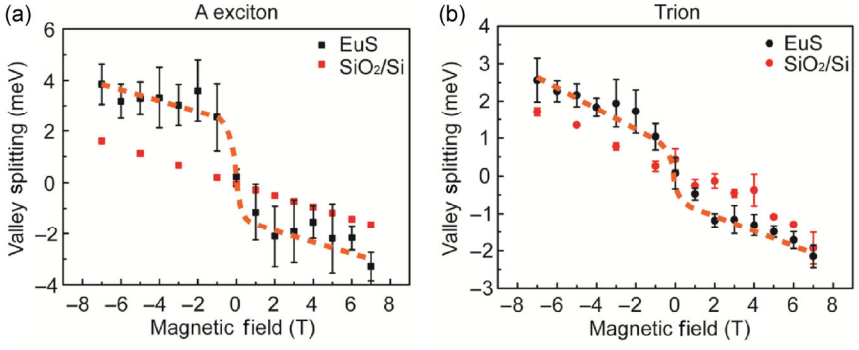

Figure 4 Valley splittings of A excitons and trions in WSe_2 on nonmagnetic and magnetic substrates. (a) Experimentally determined valley splittings of A excitons versus magnetic field in WSe_2 on nonmagnetic SiO_2/Si (red squares) and ferromagnetic EuS (black squares) are presented. The valley splitting of A excitons in WSe_2 on SiO_2/Si matches well with the expected values; while for WSe_2 on EuS, the enhanced valley splitting shows a nonlinear relationship with the external magnetic field due to the MEF between the WSe_2 and EuS. The orange guideline indicates that the enhanced valley splitting of A excitons follows the trend of field dependent magnetization of EuS. (b) Experimentally determined valley splittings of trions versus magnetic field in WSe_2 on nonmagnetic SiO_2/Si (red dots) and ferromagnetic EuS (black dots). The valley splitting of trions in WSe_2 on SiO_2/Si shows a linear relationship with the magnetic field. For WSe_2 on EuS, the enhanced valley splitting of trions shows a similar nonlinear trend as seen in A excitons of WSe_2 on EuS. Valley splittings are extracted from the PL spectra at selected magnetic fields as the difference between the peak energies of σ^+ and σ^- polarized emissions for A excitons and trions.

Table 1 Summary of the effective *g*-factors of ML WSe_2 on SiO_2/Si

Substrates	A exciton *g*-factor	Trion *g*-factor
SiO_2/Si (reference)	−3.7 ± 0.2 [25]	−4.4 ± 0.2 [25]
	−4.37 ± 0.15 [37]	−6.28 ± 0.32 [37]
	3.14 to 5.72 [16]	—
	~ 3.46 [23]	—
SiO_2/Si (in this work)	3.97 ± 0.02	4.15 ± 0.03

with the external magnetic field, and the slope is −0.24 meV/T; consequently, the effective *g*-factor can be extracted as 4.15, which is comparable with the effective *g*-factor of A excitons. The similar valley splitting behavior of A excitons and trions in ML WSe_2 on SiO_2/Si matches the theoretical calculations well [17]. In contrast, the valley splitting of trions in ML WSe_2 on EuS (black dots in Fig. 4(b)) shows significant enhancement as compared to the trions case on SiO_2/Si. The orange guideline of trions shows a similar large enhancement within $|B| < 1$ T as compared with the guideline of A excitons in WSe_2 on EuS, and increases slowly with increasing external magnetic field when $|B| > 1$ T. By comparing the valley splittings of A excitons and trions in ML WSe_2 on EuS, we find that the MEF enhances the valley splitting energies of both A excitons and trions.

The nonlinear behavior of the valley splittings of A excitons and trions in ML WSe_2 on EuS suggests that the MEF between the WSe_2 and EuS substrate is highly dependent on the magnetization of the EuS substrate [23]. For $|B| < 1$ T, the magnetization of the EuS substrate is highly sensitive to the magnetic field, resulting in greatly enhanced valley splitting energies. When $|B| > 1$ T, the magnetization slowly becomes saturated thus the valley splitting behavior is similar to the case of ML WSe_2 on SiO_2/Si.

3 Conclusion

We have performed circular-polarization-resolved magneto-PL measurements on ML WSe_2 with SiO_2/Si and EuS substrates. Valley splittings of both A excitons and trions are enhanced by the MEF resulting from the magnetic proximity effect when EuS is used as the substrate. More specifically, for $|B| < 1$ T, the valley splitting energies are greatly enhanced, whereas for $|B| > 1$ T, the valley splitting behavior is similar to the case of ML WSe_2 on SiO_2/Si. The nonlinear valley splitting enhancement of both A excitons and trions is due to the field-dependent magnetization of EuS. Based on our estimation, the value of MEF between WSe_2 and EuS is approximately 9 T. Our results

demonstrate that the valley splittings of A excitons and trions in ML WSe_2 can be controlled by changing the magnetic properties of the substrate, which can be utilized in future valleytronic devices.

Acknowledgements

This work is supported by the National Natural Science Foundation of China (No. 61774040), the National Young 1000 Talent Plan of China, the Shanghai Municipal Natural Science Foundation (No. 16ZR1402500), the Opening project of State Key Laboratory of Functional Materials for Informatics (Shanghai Institute of Microsystem and Information Technology, Chinese Academy of Sciences), Singapore Ministry of Education (MOE) Tier 1 RG199/17, NTU Start-up grant M4080513, US NSF MRI-1229208 and UB RENEW Institute. M. E. acknowledges support by Jiangsu 100 Talent and Six Categories of Talent.

References

[1] Radisavljevic, B.; Radenovic, A.; Brivio, J.; Giacometti, V.; Kis, A. Single-layer MoS_2 transistors. *Nat. Nanotechnol.* **2011**, *6*, 147–150.

[2] Jariwala, D.; Sangwan, V. K.; Lauhon, L. J.; Marks, T. J.; Hersam, M. C. Emerging device applications for semiconducting two-dimensional transition metal dichalcogenides. *ACS Nano* **2014**, *8*, 1102–1120.

[3] Wang, Q. H.; Kalantar-Zadeh, K.; Kis, A.; Coleman, J. N.; Strano, M. S. Electronics and optoelectronics of two-dimensional transition metal dichalcogenides. *Nat. Nanotechnol.* **2012**, *7*, 699–712.

[4] Lopez-Sanchez, O.; Lembke, D.; Kayci, M.; Radenovic, A.; Kis, A. Ultrasensitive photodetectors based on monolayer MoS_2. *Nat. Nanotechnol.* **2013**, *8*, 497–501.

[5] Xu, X. D.; Yao, W.; Xiao, D.; Heinz, T. F. Spin and pseudospins in layered transition metal dichalcogenides. *Nat. Phys.* **2014**, *10*, 343–350.

[6] Peimyoo, N.; Shang, J. Z.; Cong, C. X.; Shen, X. N.; Wu, X. Y.; Yeow, E. K. L.; Yu, T. Nonblinking, intense two-dimensional light emitter: Monolayer WS_2 triangles. *ACS Nano* **2013**, *7*, 10985–10994.

[7] Young, A. F.; Sanchez-Yamagishi, J. D.; Hunt, B.; Choi, S. H.; Watanabe, K.; Taniguchi, T.; Ashoori, R. C.; Jarillo-Herrero, P. Tunable symmetry breaking and helical edge transport in a graphene quantum spin Hall state. *Nature* **2014**, *505*, 528–532.

[8] Cai, T. Y.; Yang, S. A.; Li, X.; Zhang, F.; Shi, J. R.; Yao, W.; Niu, Q. Magnetic control of the valley degree of freedom of massive Dirac fermions with application to transition metal dichalcogenides. *Phys. Rev. B* **2013**, *88*, 115140.

[9] Wu, S. F.; Ross, J. S.; Liu, G. B.; Aivazian, G.; Jones, A.; Fei, Z. Y.; Zhu, W. G.; Xiao, D.; Yao, W.; Cobden, D. et al. Electrical tuning of valley magnetic moment through symmetry control in bilayer MoS_2. *Nat. Phys.* **2013**, *9*, 149–153.

[10] Sun, L. F.; Yan, J. X.; Zhan, D.; Liu, L.; Hu, H. L.; Li, H.; Tay, B. K.; Kuo, J. L.; Huang, C. C.; Hewak, D. W. et al. Spin-orbit splitting in single-layer MoS_2 revealed by triply resonant Raman scattering. *Phys. Rev. Lett.* **2013**, *111*, 126801.

[11] Zeng, H. L.; Dai, J. F.; Yao, W.; Xiao, D.; Cui, X. D. Valley polarization in MoS_2 monolayers by optical pumping. *Nat. Nanotechnol.* **2012**, *7*, 490–493.

[12] Sie, E. J.; McIver, J.; Lee, Y. H.; Fu, L.; Kong, J.; Gedik, N. Valley-selective optical Stark effect in monolayer WS_2. *Nat. Mater.* **2015**, *14*, 290–294.

[13] Zeng, H. L.; Cui, X. D. An optical spectroscopic study on two-dimensional group-VI transition metal dichalcogenides. *Chem. Soc. Rev.* **2015**, *44*, 2629–2642.

[14] Mak, K. F.; He, K. L.; Shan, J.; Heinz, T. F. Control of valley polarization in monolayer MoS_2 by optical helicity. *Nat. Nanotechnol.* **2012**, *7*, 494–498.

[15] Yao, W.; Xiao, D.; Niu, Q. Valley-dependent optoelectronics from inversion symmetry breaking. *Phys. Rev. B* **2008**, *77*, 235406.

[16] Aivazian, G.; Gong, Z. R.; Jones, A. M.; Chu, R. L.; Yan, J.; Mandrus, D. G.; Zhang, C. W.; Cobden, D.; Yao, W.; Xu, X. Magnetic control of valley pseudospin in monolayer WSe_2. *Nat. Phys.* **2015**, *11*, 148–152.

[17] MacNeill, D.; Heikes, C.; Mak, K. F.; Anderson, Z.; Kormányos, A.; Zólyomi, V.; Park, J.; Ralph, D. C. Breaking of valley degeneracy by magnetic field in monolayer $MoSe_2$. *Phys. Rev. Lett.* **2015**, *114*, 037401.

[18] Li, Y. L.; Ludwig, J.; Low, T.; Chernikov, A.; Cui, X.; Arefe, G.; Kim, Y. D.; van der Zande, A. M.; Rigosi, A.; Hill, H. M. et al. Valley splitting and polarization by the Zeeman effect in monolayer $MoSe_2$. *Phys. Rev. Lett.* **2014**, *113*, 266804.

[19] Arora, A.; Schmidt, R.; Schneider, R.; Molas, M. R.; Breslavetz, I.; Potemski, M.; Bratschitsch, R. Valley Zeeman splitting and valley polarization of neutral and charged excitons in monolayer $MoTe_2$ at high magnetic fields. *Nano Lett.* **2016**, *16*, 3624–3629.

[20] Mitioglu, A. A.; Plochocka, P.; Granados del Aguila, A.; Christianen, P. C. M.; Deligeorgis, G.; Anghel, S.; Kulyuk, L.; Maude, D. K. Optical investigation of monolayer and bulk tungsten diselenide (WSe_2) in high magnetic fields. *Nano Lett.* **2015**, *15*, 4387–4392.

[21] Stier, A. V.; McCreary, K. M.; Jonker, B. T.; Kono, J.; Crooker, S. A. Exciton diamagnetic shifts and valley Zeeman effects in monolayer WS_2 and MoS_2 to 65 Tesla. *Nat. Commun.* **2016**, *7*, 10643.

[22] Wei, P.; Lee, S.; Lemaitre, F.; Pinel, L.; Cutaia, D.; Cha, W.; Katmis, F.; Zhu, Y.; Heiman, D.; Hone, J. et al. Strong interfacial exchange field in the graphene/EuS heterostructure. *Nat. Mater.* **2016**, *15*, 711–716.

[23] Zhao, C.; Norden, T.; Zhang, P. Y.; Zhao, P. Q.; Cheng, Y. C.; Sun, F.; Parry, J. P.; Taheri, P.; Wang, J. Q.; Yang, Y. H. et al. Enhanced valley splitting in monolayer WSe_2 due to magnetic exchange field. *Nat. Nanotechnol.* **2017**, *12*, 757–762.

[24] Xiao, D.; Liu, G. B.; Feng, W. X.; Xu, X. D.; Yao, W. Coupled spin and valley physics in monolayers of MoS_2 and other group-VI dichalcogenides. *Phys. Rev. Lett.* **2012**, *108*, 196802.

[25] Wang, G.; Bouet, L.; Glazov, M. M.; Amand, T.; Ivchenko, E. L.; Palleau, E.; Marie, X.; Urbaszek, B. Magneto-optics in transition metal diselenide monolayers. *2D Mater.* **2015**, *2*, 034002.

[26] Li, H.; Lu, G.; Wang, Y. L.; Yin, Z. Y.; Cong, C. X.; He, Q. Y.; Wang, L.; Ding, F.; Yu, T.; Zhang, H. Mechanical exfoliation and characterization of single- and few-layer nanosheets of WSe_2, TaS_2, and $TaSe_2$. *Small* **2013**, *9*, 1974–1981.

[27] Sahin, H.; Tongay, S.; Horzum, S.; Fan, W.; Zhou, J.; Li, J.; Wu, J.; Peeters, F. M. Anomalous Raman spectra and thickness-dependent electronic properties of WSe_2. *Phys. Rev. B* **2013**, *87*, 165409.

[28] Rice, C.; Young, R. J.; Zan, R.; Bangert, U.; Wolverson, D.; Georgiou, T.; Jalil, R.; Novoselov, K. S. Raman-scattering measurements and first-principles calculations of strain-induced phonon shifts in monolayer MoS_2. *Phys. Rev. B* **2013**, *87*, 081307.

[29] Wang, Y. L.; Cong, C. X.; Yang, W. H.; Shang, J. Z.; Peimyoo, N.; Chen, Y.; Kang, J. Y.; Wang, J. P.; Huang, W.; Yu, T. Strain-induced direct–indirect bandgap transition and phonon modulation in monolayer WS_2. *Nano Res.* **2015**, *8*, 2562–2572.

[30] Liu, Q.; Peng, F. Elasticity and thermodynamic properties of EuS related to phase transition. *Chin. J. Chem. Phys.* **2014**, *27*, 387–393.

[31] Morell, N.; Reserbat-Plantey, A.; Tsioutsios, I.; Schadler, K. G.; Dubin, F.; Koppens, F. H.; Bachtold, A. High quality factor mechanical resonators based on WSe_2 monolayers. *Nano Lett.* **2016**, *16*, 5102–5108.

[32] Tada, H.; Kumpel, A. E.; Lathrop, R. E.; Slanina, J. B.; Nieva, P.; Zavracky, P.; Miaoulis, I. N.; Wong, P. Y. Thermal expansion coefficient of polycrystalline silicon and silicon dioxide thin films at high temperatures. *J. Appl. Phys.* **2000**, *87*, 4189–4193.

[33] Chakraborty, B.; Bera, A.; Muthu, D. V. S.; Bhowmick, S.; Waghmare, U. V.; Sood, A. K. Symmetry-dependent phonon renormalization in monolayer MoS_2 transistor. *Phys. Rev. B* **2012**, *85*, 161403.

[34] Müller, N.; Eckstein, W.; Heiland, W.; Zinn, W. Electron spin polarization in field emission from EuS-coated tungsten tips. *Phys. Rev. Lett.* **1972**, *29*, 1651–1654.

[35] Britnell, L.; Ribeiro, R. M.; Eckmann, A.; Jalil, R.; Belle, B. D.; Mishchenko, A.; Kim, Y. J.; Gorbachev, R. V.; Georgiou, T.; Morozov, S. V. et al. Strong light-matter interactions in heterostructures of atomically thin films. *Science* **2013**, *340*, 1311–1314.

[36] Tosun, M.; Chuang, S.; Fang, H.; Sachid, A. B.; Hettick, M.; Lin, Y. J.; Zeng, Y. P.; Javey, A. High-gain inverters based on WSe_2 complementary field-effect transistors. *ACS Nano* **2014**, *8*, 4948–4953.

[37] Srivastava, A.; Sidler, M.; Allain, A. V.; Lembke, D. S.; Kis, A.; Imamoğlu, A. Valley Zeeman effect in elementary optical excitations of monolayer WSe_2. *Nat. Phys.* **2015**, *11*, 141–147.

[38] Jones, A. M.; Yu, H. Y.; Ghimire, N. J.; Wu, S. F.; Aivazian, G.; Ross, J. S.; Zhao, B.; Yan, J. Q.; Mandrus, D. G.; Xiao, D. et al. Optical generation of excitonic valley coherence in monolayer WSe_2. *Nat. Nanotechnol.* **2013**, *8*, 634–638.

[39] Huang, J.; Hoang, T. B.; Mikkelsen, M. H. Probing the origin of excitonic states in monolayer WSe_2. *Sci. Rep.* **2016**, *6*, 22414.

[40] You, Y. M.; Zhang, X.-X.; Berkelbach, T. C.; Hybertsen, M. S.; Reichman, D. R.; Heinz, T. F. Observation of biexcitons in monolayer WSe_2. *Nat. Phys.* **2015**, *11*, 477–481.

[41] Desai, S. B.; Seol, G.; Kang, J. S.; Fang, H.; Battaglia, C.; Kapadia, R.; Ager, J. W.; Guo, J.; Javey, A. Strain-induced indirect to direct bandgap transition in multilayer WSe_2. *Nano Lett.* **2014**, *14*, 4592–4597.

[42] Yun, W. S.; Han, S. W.; Hong, S. C.; Kim, I. G.; Lee, J. D. Thickness and strain effects on electronic structures of transition metal dichalcogenides: 2H-MX_2 semiconductors (M = Mo, W; X = S, Se, Te). *Phys. Rev. B* **2012**, *85*, 033305.